

ARTICLE

DOI: 10.1038/s41467-018-03418-2

OPEN

Identification of single amino acid differences in uniformly charged homopolymeric peptides with aerolysin nanopore

Fabien Piguet¹, Hadjer Ouldali¹, Manuela Pastoriza-Gallego¹, Philippe Manivet^{2,3}, Juan Pelta⁴ & Abdelghani Oukhaled¹

There are still unmet needs in finding new technologies for biomedical diagnostic and industrial applications. A technology allowing the analysis of size and sequence of short peptide molecules of only few molecular copies is still challenging. The fast, low-cost and label-free single-molecule nanopore technology could be an alternative for addressing these critical issues. Here, we demonstrate that the wild-type aerolysin nanopore enables the size-discrimination of several short uniformly charged homopeptides, mixed in solution, with a single amino acid resolution. Our system is very sensitive, allowing detecting and characterizing a few dozens of peptide impurities in a high purity commercial peptide sample, while conventional analysis techniques fail to do so.

¹LAMBE UMR 8587, Université de Cergy-Pontoise, 95300 Pontoise, France. ²APHP, Centre de Ressources Biologiques BB-0033-00064, Plateforme de Bio-Pathologie et de Technologies Innovantes en santé, Hôpital Lariboisière, 75010 Paris, France. ³INSERM UMR-S942, Hôpital Lariboisière, 75010 Paris, France. ⁴LAMBE UMR 8587, Université d'Evry-Val-d'Essonne, 91000 Evry, France. These authors contributed equally: Fabien Piguet, Hadjer Ouldali. Correspondence and requests for materials should be addressed to F.P. (email: fabien.piguet@u-cergy.fr) or to J.P. (email: juan.pelta@univ-evry.fr) or to A.O. (email: abdelghani.oukhaled@u-cergy.fr)

Recently, the concept of personalized medicine has evolved towards the analysis of rare cells (tumor and endothelial cells, cancer stem cells, etc.) and extracellular vesicles circulating in the blood, containing a few copies of biomarkers. Among the biomarkers there are short signal peptides that are able to modulate the cancer cells aggressiveness more or less upon their ability to be processed by proteolysis driven by N-end rules pathways¹. Classical metabolomics and proteomics techniques, such as mass spectrometry (MS), High Performance Liquid Chromatography (HPLC), or Nuclear Magnetic Resonance (NMR), suffer a lack of reproducibility and sensitivity that prohibit their use for medical diagnostic^{2,3}. In addition, these techniques are too expensive, time consuming and heavy to handle in the view of developing a portable medical device application³. In the industry context, pharmaceutical peptides manufacturing requires a high purity level and is still waiting for high-sensitivity analytical methods addressing Good Manufacturing Practice issues such as impurities profile characterization⁴. Nanopore single-molecule technology⁵ seems to be an excellent alternative for addressing the above issues. For more than two decades, the nanopore technology has been essentially applied to DNA⁶. The development of nanopore-based DNA sequencing is now achieved and commercialized. The current challenge is the application of nanopore technology to peptides and proteins identification, fingerprinting and sequencing.

To date, nanopores were successfully used to detect protein or peptides either through biological nanopores^{7–39} or through artificial nanopores^{40–59}. Protein or peptides were probed either inside a natural nanopore^{21,29,35} or outside a natural nanopore with an aptamer^{21,22} or with a ligand⁷. Pioneering studies were devoted to the dynamics of peptides transport^{9,10,13,14,16,30}, and then to the dynamics of unfolded proteins transport^{18,31,48} through the nanopore. Others studies focused on protein-antibodies complex^{32,41,42}, on intrinsically disordered proteins⁴⁹, on enzymatic reactions^{15,17,23,60,61} and on the aggregation of amyloidogenic peptides^{36,47,55}. The unfolding of proteins was investigated, either in the presence of an unfolding agent^{12,31,44}, or by varying temperature²⁴, or with an electrical force^{50,62}, or with a molecular motor such as an unfoldase²⁷. Nanopores were also used to study the structure of peptides⁸, conformational changes of proteins^{12,39,44,54,57}, post-translational modification of proteins^{52,58} and to estimate the shape, volume, charge, rotational diffusion coefficient and dipole moment of individual proteins⁶³.

In the context of nanopore-based protein sizing, glass nanopores were used to determine folded protein sizes ranging from 12 to 480 kDa^{51,53}. The best discrimination resolution obtained with this approach was a difference of 4 kDa in the case of the shortest proteins, and a difference of 50 kDa in the case of the longest proteins^{51,53}. Then solid-state nanopores were demonstrated to enable the detection of proteins as small as 8.5 kDa⁵⁴ and the discrimination between two different proteins with a resolution of 1.7 kDa⁵⁷. Regarding biological nanopores, Fraga-toxin C (FraC) channels were recently successfully used to discriminate peptides and proteins as a model biomarkers ranging from 25 kDa down to 1.3 kDa³⁸. In the same context, α -hemolysin nanopore equipped with Au₂₅(SG)₁₈ clusters was used to increase the on-rate and off-rate of peptides to the pore in order to improve the mass resolution of the nanopore sensor³⁷. Thus, while biological nanopores were previously used for size-discriminating DNA hairpins⁶⁴, synthetic polymers^{65–67} and oligonucleotides⁶⁸ with monomeric resolution, the single-amino-acid size-discrimination between several (more than two) peptides mixed in solution that differ by a single amino acid and the characterization of rare peptide impurities were not demonstrated, regardless of the pore used^{9,10,20,30,37,38,65,66,68}. In previous works using biological nanopores, there was no more than

two peptides differing by one amino acid among the different peptides used^{10,37,38}.

Here, we demonstrate the proof-of-concept of size-discrimination of short uniformly charged homopeptides, mixed in solution or independently, with a single amino acid resolution by using the recombinant aerolysin nanopore without any physical or chemical modifications. The sensitivity of this pore allows detecting, with a single amino acid resolution, peptide fragments of different lengths present in a high purity commercial peptide sample. We also show the discrimination between two homopolymeric- and one heteropolymeric peptides having the same length. Our system also enables the real-time monitoring of the evolution of the peptide populations with a single amino acid resolution during the enzymatic degradation of a peptide sample. These findings open new perspectives, in particular towards the use of nanopore technology for the size-discrimination and sequence recognition of peptides and proteins.

Results

Single amino acid resolution size-discrimination of peptides. A schematic of the experimental setup is shown in Fig. 1a. A single wild-type aerolysin nanopore was inserted in a lipid bilayer separating the *cis*-compartments and *trans*-compartments filled with an electrolyte solution. An external voltage was applied on the *trans*-side of the bilayer, the *cis*-side being at voltage ground. In absence of analytes, a stable ionic current of mean value I_0 flowing through the nanopore was measured. The addition of an equimolar mixture of arginine peptides of 6 different lengths differing by a single amino acid in length (5, 6, 7, 8, 9, 10 amino acids) on the *cis*-side of the bilayer induced well-resolved current blockades of different amplitudes and durations under a negative applied voltage (Fig. 1a,c), in agreement with the positive electrical charge of arginine peptides under our experimental conditions. In contrast, no current blockades were observed either when the peptides were added on the *cis*-side under a positive applied voltage, or when the peptides were added on the *trans*-side regardless of the voltage polarity (Supplementary Fig. 1).

The histogram of the relative blockade current I_b/I_0 values induced by the mixture of arginine peptides of 6 different lengths is shown in Fig. 1d. Well-separated peaks corresponding to distinct populations with preferred I_b/I_0 values are observed. For each of the 6 main populations, the mean relative blockade current is (mean value of a gaussian fit of the peak \pm one standard deviation): 0.234 \pm 0.001, 0.286 \pm 0.002, 0.353 \pm 0.002, 0.435 \pm 0.002, 0.530 \pm 0.002, 0.631 \pm 0.004. The interval between two consecutive peaks is at least 25-fold greater than the peaks widths. The mean blockade duration of each population increases by almost two orders of magnitude as the relative blockade current value decreases, from 0.9 ms for the shallowest population to 72 ms for the deepest population.

In order to ascertain whether the different populations observed in the I_b/I_0 histogram correspond to the different peptide lengths present in the arginine peptide mixture, experiments probing independently the interaction of arginine peptides of each individual length (5, 6, 7, 8, 9, 10 amino acids) with the aerolysin nanopore were performed under the same experimental conditions. The histograms of the relative blockade current I_b/I_0 values corresponding to each of the 6 different peptide lengths are shown in Fig. 2b–g. Each histogram shows an overwhelming majority population with a preferred I_b/I_0 value, corresponding to the peptide length used. The location of the majority population depends on the peptide length: the mean I_b/I_0 value of the majority population decreases as the peptide length increases. Comparing with the I_b/I_0 histogram of the peptide mixture (Fig. 2a) reveals that each majority population

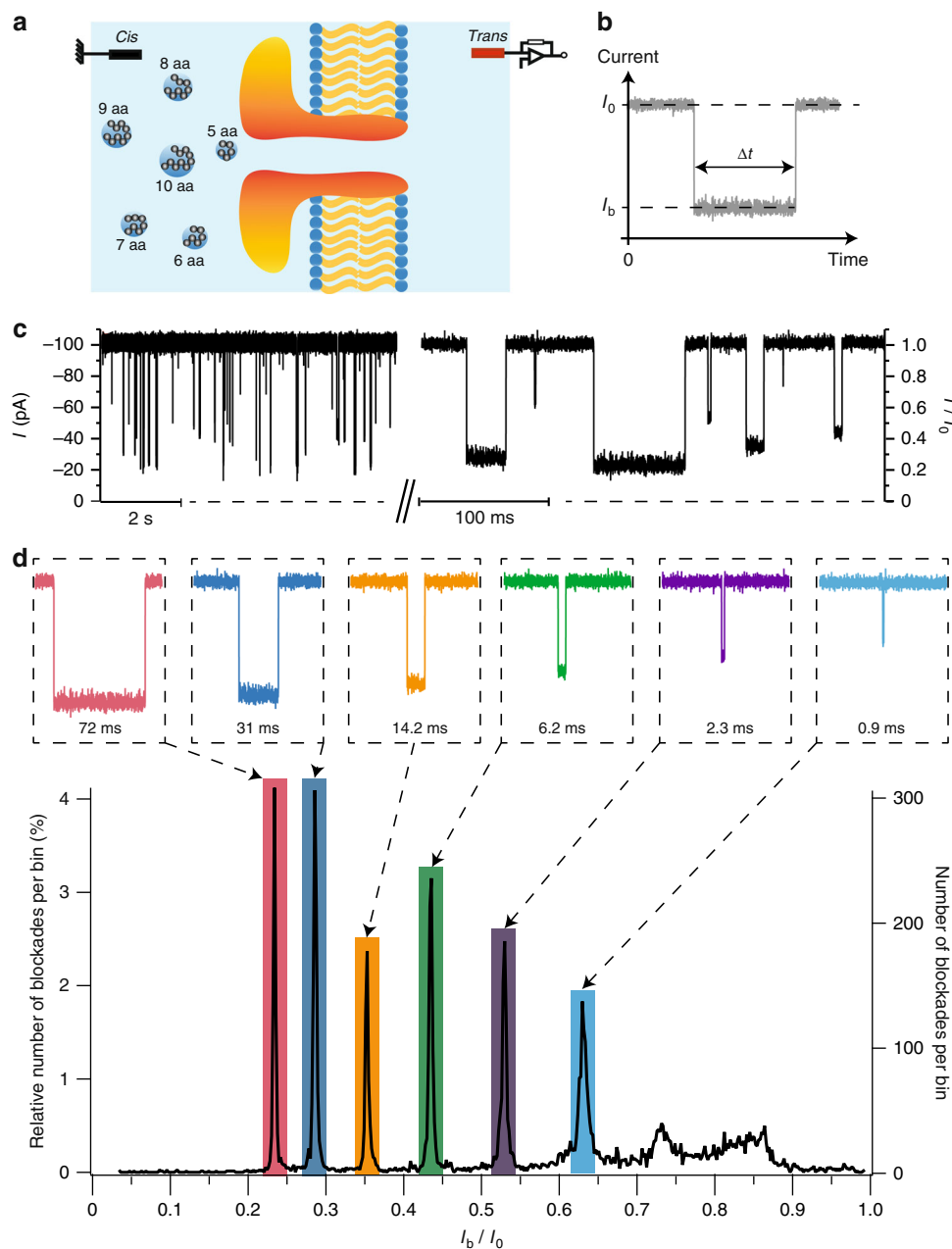


Fig. 1 Detection of a mixture of arginine peptides of different lengths. **a** Schematics of the experimental setup (not to scale). A single wild-type aerolysin nanopore was inserted in a lipid bilayer separating the *cis*- and *trans*-compartments filled with an electrolyte solution. An external voltage was applied on the *trans*-side of the bilayer, the *cis*-side being at voltage ground. A mixture of arginine peptides of different lengths (5, 6, 7, 8, 9, and 10 amino acids) was added on the *cis*-side of the bilayer. **b** Illustration of a typical current blockade event. The interaction of a peptide with the nanopore is detected as a partial and temporary blockade of the electrical current flowing through the nanopore from its open-pore current value I_0 to the blockade current value I_b . The current blockade duration Δt corresponds to the duration of the peptide/nanopore interaction. **c** Portion of a typical current versus time recording through aerolysin nanopore in presence of an equimolar mixture (1 μ M) of arginine peptides of different lengths (5, 6, 7, 8, 9, and 10 amino acids) in KCl 4 M HEPES 5 mM pH = 7.5 at -50 mV and at 20 °C. The left axis indicates the current I values (negative current values under a negative applied voltage) and the right axis indicates the relative current I/I_0 values. An enlargement of the current trace shows typical current blockades of different amplitudes and durations. **d** Histogram of the relative blockade current I_b/I_0 values corresponding to the current trace in (c). The right axis indicates the number of blockades per bin and the left axis indicates the relative number of blockades per bin (i.e., the ratio of the number of blockades per bin on the total number of blockades). The histogram reveals the existence of at least 6 distinct populations corresponding to preferred relative blockade current values. Inserts on the top show a typical current blockade event and indicate the mean blockade duration for each population

corresponding to a given peptide length coincides with one of the main populations observed in the mixture histogram. This enables to attribute an individual peptide length to each population observed in the mixture histogram, from 10 amino acids long arginine peptides for the deepest population ($I_b/I_0 =$

0.234) to 5 amino acids long arginine peptides for the shallowest population ($I_b/I_0 = 0.631$). This demonstrates the ability of the wild-type aerolysin nanopore to perform the size-discrimination of arginine peptides with a single amino acid resolution. Furthermore, measurements of the mean relative blockade

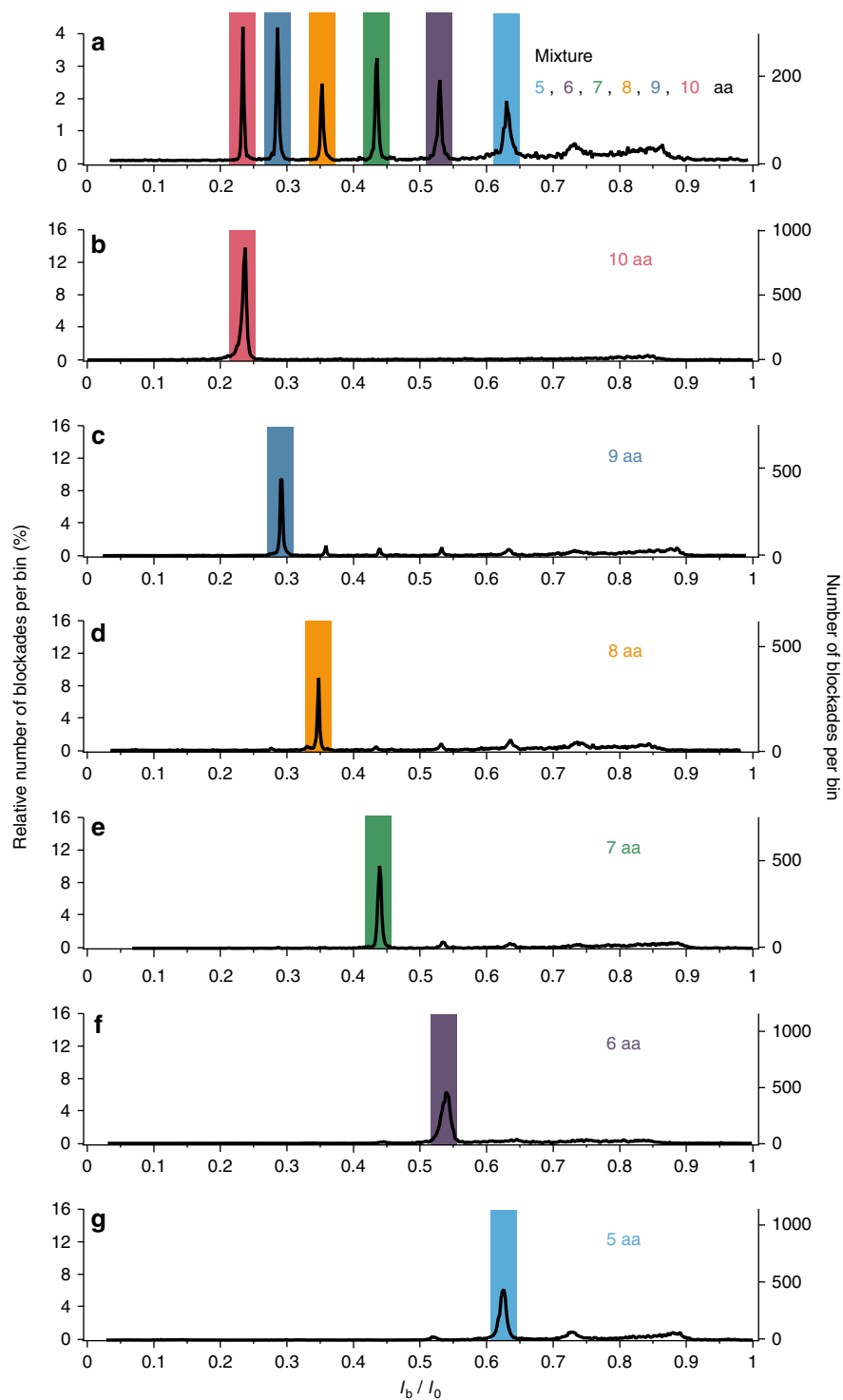


Fig. 2 Size-discrimination of arginine peptides with a single amino acid resolution. Histograms of the relative blockade current I_b/I_0 values in the case of the interaction of aerolysin nanopore with: **a** an equimolar mixture of arginine peptides of different lengths (5, 6, 7, 8, 9, and 10 amino acids), a solution of 10 (**b**), 9 (**c**), 8 (**d**), 7 (**e**), 6 (**f**), and 5 (**g**) amino acids long arginine peptides. Each histogram corresponding to a given peptide length (from **b-g**) exhibits a single I_b/I_0 population which also appears in the mixture histogram (**a**), allowing to discriminate and identify the peptides of different lengths in the mixture with a single amino acid resolution. The data were acquired in KCl 4 M HEPES 5 mM pH = 7.5 at -50 mV and at 20°C

current value and of the mean blockade duration corresponding to each individual peptide length are highly reproducible between independent experiments (Supplementary Fig. 2), highlighting the high-fidelity resolution power of the nanopore.

The effect of voltage on the interaction of the aerolysin nanopore with a mixture of arginine peptides of 6 different

lengths (5 to 10 amino acids) is shown in Supplementary Figs. 3 and 4, for negative voltages ranging from -25 to -80 mV. For each voltage, the populations corresponding to the different peptide lengths in the mixture were identified from the I_b/I_0 histogram (Supplementary Fig. 4) and independently analyzed (see the Methods section). Regardless of the applied voltage, the

mean blockade duration increases with the peptide length, up to two orders of magnitude between 5 amino acids long and 10 amino acids long peptides (Supplementary Fig. 3b). For each peptide length, the mean blockade duration depends non-monotonically on voltage, first increasing with voltage magnitude, reaching a maximum and then decreasing. The voltage corresponding to the maximum of the mean blockade duration depends only slightly on the peptide length, if at all, and is comprised between -35 and -40 mV. Note that the mean blockade duration corresponding to each peptide length are identical when measured whether in a peptide mixture experiment or in independent experiments for each peptide length.

The qualitative voltage dependence of the mean relative blockade current I_b/I_0 depends on the arginine peptide length (Supplementary Figs. 3a and 4): the mean I_b/I_0 slightly decreases with voltage magnitude for the longest peptides (10, 9, and 8 amino acids), is voltage-independent for intermediate peptide lengths (7 and 6 amino acids) and even slightly increases with voltage magnitude for the shortest peptides (5 amino acids). As shown in the I_b/I_0 histograms of the peptide mixture under different applied voltages (Supplementary Fig. 4), the size-discrimination of arginine peptides of different lengths with a single amino acid resolution is preserved in the whole voltage range explored, even at a voltage as low as -25 mV. Note that maximizing the mean blockade duration for each of the different peptide lengths (at ≈ -40 mV) does not maximize the size-discrimination power of the nanopore. Interestingly, the different populations of the I_b/I_0 histogram of the peptide mixture become increasingly separated as the negative voltage magnitude increases. For voltage magnitudes greater than or equal to -50 mV (Supplementary Fig. 4 and Fig. 1d), an additional population with a mean $I_b/I_0 \approx 0.73$ appeared. This additional population is the 7th population detected from an arginine peptide mixture of 6 different lengths, and is located in the short peptide part of the I_b/I_0 histogram. Observing this additional population was not possible at low voltages, probably due to the presence of a significant number of current fluctuations from the residual open pore current noise, with I_b/I_0 values between ≈ 0.7 and 0.8 . As the voltage magnitude is increased, the signal-to-noise ratio is enhanced ($I_b/I_0 = 0.83$ at -25 mV and 0.91 at -80 mV, I_0 and σ being the mean open pore current and its standard deviation respectively, see the Methods section and Supplementary Fig. 8 for details); current fluctuations due to residual open pore current noise are shifted to greater I_b/I_0 values with increasing voltage magnitude, enabling the clear observation of the additional population whose identification is established in the next section.

Detection and identification of peptide impurities. The histogram of the relative blockade current I_b/I_0 values and the scatter plot of blockade duration as a function of the relative blockade current are shown in Fig. 3b in the case of the interaction of a high-purity arginine peptide sample ($>98\%$ purity in peptide length) of given length (9 amino acids) with the aerolysin nanopore. As already observed in Fig. 2c, the I_b/I_0 histogram shows an overwhelming majority population corresponding to the 9 amino acids peptide length used. In addition to the majority population, at least four minority populations are detected. Each peak of the I_b/I_0 histogram corresponds to a distinct line-shaped cluster of dots in the scatter plot of blockade duration as a function of the relative blockade current, showing the different populations, and in particular the minority populations, even more clearly. Comparing with the case of the interaction of an equimolar mixture of arginine peptides of 6 different lengths (5 to 10 amino acids) with the aerolysin nanopore (Fig. 3a) reveals that the minority populations detected in the high-purity 9 amino

acids long arginine peptide sample correspond to arginine peptide fragments whose length can be identified (5, 6, 7, 8 amino acids). Interestingly, quantities as small as a few dozens of molecules are detected for each peptide fragment length (see the right axis of the I_b/I_0 histogram in Fig. 3b), revealing the high sensitivity of the nanopore system. In contrast, the purity analysis provided by the peptide supplier using conventional techniques (High Purity Liquid Chromatography, HPLC, and Mass Spectrometry, MS) did not identify these peptide fragments, including them among general impurities (Supplementary Fig. 5). This demonstrates that the aerolysin nanopore enables the detection, identification and quantification of the peptide impurities present in a high-purity peptide sample with a higher sensitivity than the conventional purity analysis techniques (HPLC and MS).

As already observed in the arginine peptide mixture analysis for negative voltage magnitudes greater than or equal to -50 mV (Fig. 1d and Supplementary Fig. 4), an additional and unidentified population exists in the analysis of the high-purity 9 amino acids long arginine peptide sample, located on the short-peptides side ($I_b/I_0 \approx 0.73$) (Fig. 3b). In order to ascertain whether this additional population was an artifact from the experimental setup or corresponded to analytes in solution (e.g. 4 amino acids long arginine peptides present as impurities), experiments monitoring the real-time enzymatic degradation of arginine peptides were performed. The histograms of the relative blockade current I_b/I_0 values and the scatter plots of blockade duration as a function of the relative blockade current are shown in Fig. 4 in the case of the interaction of a 9 amino acids long arginine peptide sample with the aerolysin nanopore in absence of trypsin enzyme (Fig. 4a), 10 min after trypsin addition (Fig. 4b) and 3 h 30 min after trypsin addition (Fig. 4c). As time increases, the number of current blockades corresponding to long peptides decreases while the number of current blockades corresponding to shorter peptides increases, indicating the enzymatic cleavage of long peptides into shorter ones. In particular, the population located at $I_b/I_0 \approx 0.73$ increases with time, revealing that this population, observed here and in previous Figures (Figs. 1d and 3b and Supplementary Fig. 4) corresponds to 4 amino acids long arginine peptides. Furthermore, the population located at $I_b/I_0 \approx 0.84$ increases with time, suggesting that this population could correspond to 3 amino acids long arginine peptides. This is confirmed by an independent experiment using a solution of 3 amino acids long arginine peptides (Supplementary Fig. 10).

Discrimination between lysine and arginine peptides. In order to ascertain whether the above-described method could be used with other peptides than arginine peptides, experiments probing the interaction of lysine peptides with the aerolysin nanopore were performed.

The histograms of the relative blockade current I_b/I_0 values and the scatter plots of blockade duration as a function of the relative blockade current are shown in Fig. 5 in the case of the interaction of a high-purity ($>98\%$) 10 amino acids long lysine peptide sample with the aerolysin nanopore in absence of trypsin enzyme (Fig. 5a), 30 min after trypsin addition (Fig. 5b) and 1 h 45 min after trypsin addition (Fig. 5c). Before trypsin addition (Fig. 5a), the I_b/I_0 histogram shows an overwhelming majority population, corresponding to the 10 amino acids lysine peptide length used, and additional minority populations, as in the case of arginine peptides. Moreover, as time increases after trypsin addition (Fig. 5b,c), the number of current blockades corresponding to long lysine peptides decreases while the number of current blockades corresponding to shorter lysine peptides increases, indicating the enzymatic cleavage of long lysine peptides into shorter ones, as in the case of arginine peptides. This observation

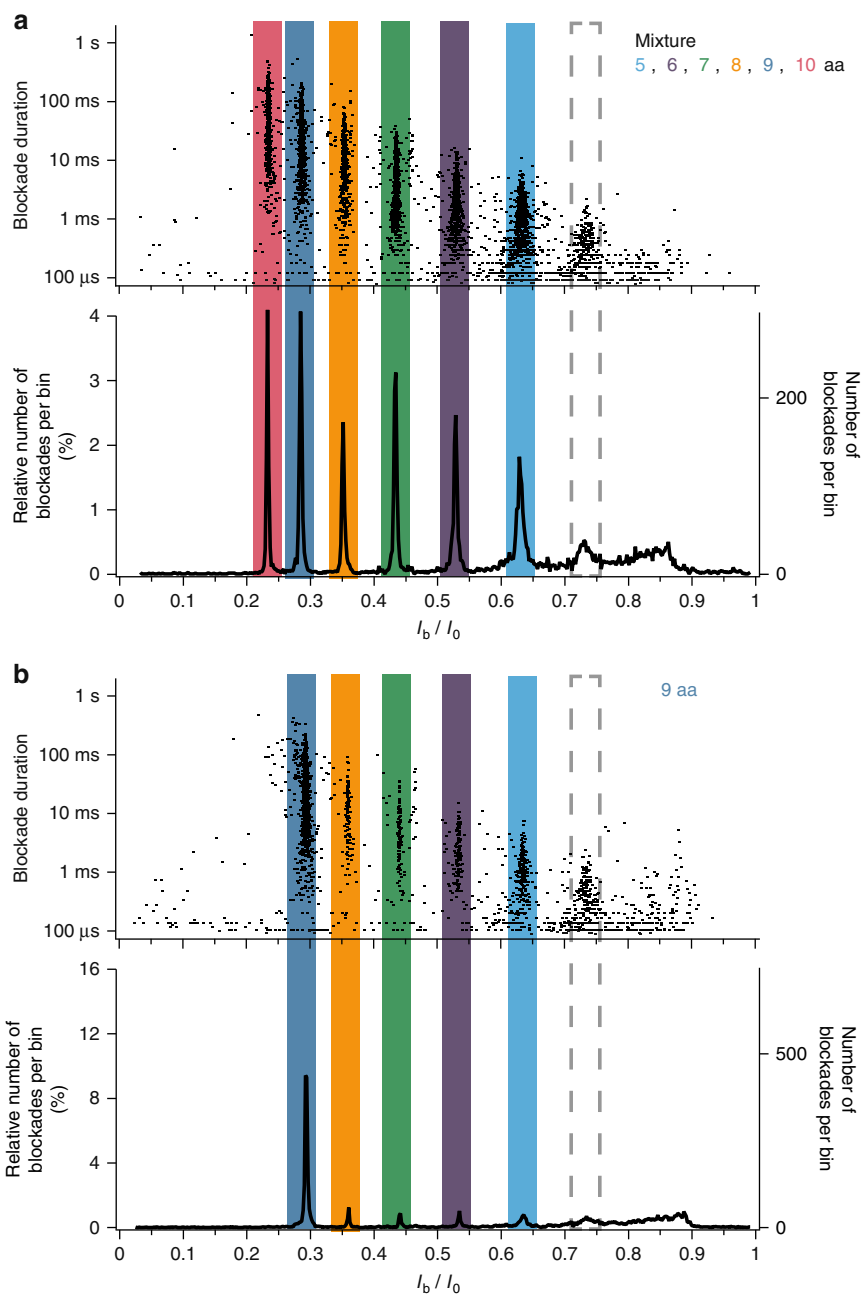


Fig. 3 High sensitivity detection and identification of peptide impurities. **a** Interaction of aerolysin nanopore with an equimolar mixture of arginine peptides of different lengths (5, 6, 7, 8, 9, and 10 amino acids): (top) scatter plot of blockade duration versus relative blockade current I_b/I_0 (every dot corresponds to a single current blockade event); (bottom) histogram of the relative blockade current I_b/I_0 values. **b** Interaction of aerolysin nanopore with a solution of 9 amino acids long arginine peptides with a >98% purity in peptide length (purity value provided by the supplier): (top) scatter plot of blockade duration versus relative blockade current I_b/I_0 (every dot corresponds to a single current blockade event); (bottom) histogram of the relative blockade current I_b/I_0 values. In **(b)**, in addition to the main population of 9 amino acids long peptides (dark blue), at least 4 minority populations of only a few dozens of molecules each are detected and identified as corresponding to 8 (yellow), 7 (green), 6 (purple), and 5 (light blue) amino acids long peptides. Another population (gray dashed rectangles) is detected at $I_b/I_0 = 0.731 \pm 0.004$ both in the peptide mixture **(a)** and in the 9 amino acids long peptides sample **(b)**. The data were acquired in KCl 4 M HEPES 5 mM pH = 7.5 at -50 mV and at 20°C

is an important indicator of the ability of the wild-type aerolysin nanopore to perform the size-discrimination of lysine peptides.

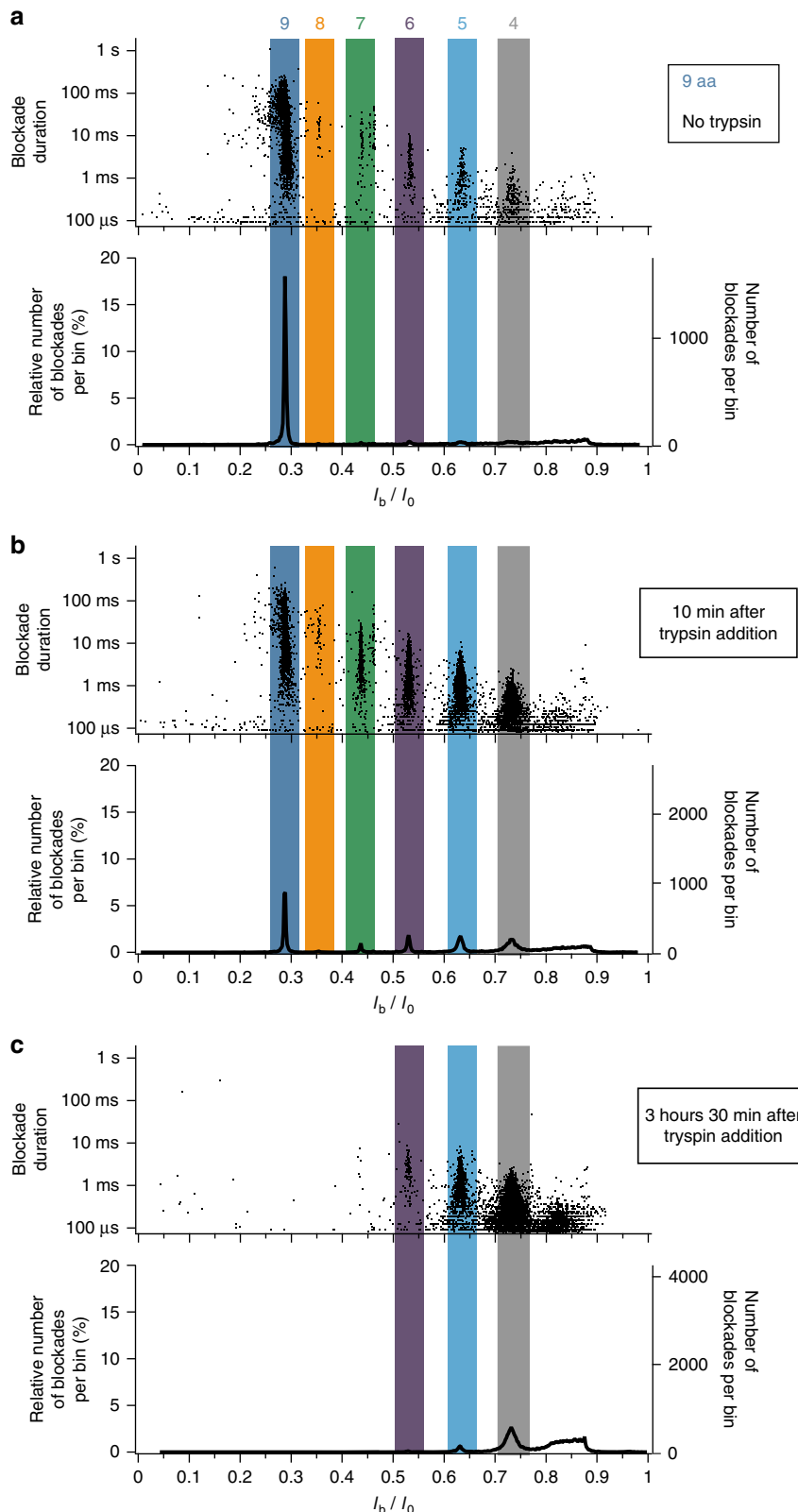
The histograms of the relative blockade current I_b/I_0 values and the scatter plots of blockade duration as a function of the relative blockade current are shown in Fig. 6 in the case of the interaction of the aerolysin nanopore with a high-purity (>98%) sample of 10 amino acids long arginine peptides (Fig. 6a) and of 10 amino acids long lysine peptides (Fig. 6c). Interestingly, the observed

majority population clearly differs between the two different peptides, both in term of mean I_b/I_0 value and in term of mean blockade duration. The mean I_b/I_0 value is 0.236 ± 0.003 in the case of arginine and 0.377 ± 0.004 in the case of lysine, while the mean blockade duration decreases by almost two orders of magnitude from nearly 100 ms in the case of arginine to nearly 1 ms in the case of lysine (see also Supplementary Fig. 7). This reveals that our method enables the discrimination between

arginine and lysine homopeptides of same length, even while arginine and lysine amino acids have the same electrical charge and very similar chemical structures.

Moreover, experiments probing the interaction of the aerolysin nanopore with a high-purity (>98%) sample of 10 amino acids long heteropeptides formed by a sequence of 5 lysine amino acids coupled to 5 arginine amino acids (Fig. 6b) reveal that this

peptide can also be discriminated from 10 amino acids long arginine peptides and from 10 amino acids long lysine peptides (Fig. 6a–c and Supplementary Fig. 7), highlighting the high-sensitivity of our method. In the case of 10 amino acids long lysine/arginine heteropeptides, the mean I_b/I_0 value is 0.297 ± 0.003 and the mean blockade duration is nearly 10 ms.



Discussion

The high resolution of aerolysin pore for the highly-sensitive analysis of short peptides is most likely attributed to its geometry, to its highly charged pore wall and to the high affinity between aerolysin and peptides (see Supplementary Fig. 6). Nanopore-based single amino acid size-discrimination of several peptide lengths mixed in solution that differ by a single amino acid is subject to four conditions: i) the whole peptide must be entirely fitted en bloc inside the vicinity of the pore, ii) all amino acids must contribute individually to the current blockades, iii) a high size-sensitivity of the pore conductance change and iv) a high affinity between the pore and the peptide (the life time of the peptide/pore interaction must exceed 2 times the rise time of the bandwidth). In our experiments, observing different residual blockade currents in the case of peptides differing by only one amino acid indicates that each amino acid contributes individually to the current blockade, corresponding to a coil or to a compact conformation of the peptide in the nanopore and not to a rod-like conformation of the peptide. In the hypothesis of a rod-like conformation of the peptide, it is expected that current blockades would only weakly, if at all, depend on the peptide length. A coil or compact conformation of the peptide is not surprising in the high salt conditions of our experiments and considering the short persistence length of peptides (≈ 2 amino acids)⁶⁹. Concerning peptides longer than 10 amino acids, experiments performed with 12 amino acids long arginine homopeptides (Supplementary Fig. 11) display a distinct preferential residual blockade current population corresponding to this peptide length, as observed for shorter peptides. Our perspectives are rather turned towards the analysis of short peptides, as short as a single amino acid, which is of particular importance towards peptide/protein sequencing. Furthermore, short peptides are widely used by cells for their communications in normal and pathologic conditions. These short peptides can be found either in the intracellular or extracellular compartments and some of them are secreted or released into extracellular vesicles, assuming functions both inside and outside the cell. Otherwise, for industrial applications, our proof-of-concept method could be extended to longer homopeptides of different chemical nature by using larger biological nanopores such as ClyA nanopore²⁸. Under appropriate experimental conditions, our proof-of-concept method could be also extended to the size-discrimination and purity analysis of other short homopeptides and heteropeptides. A possible way out would be to use low³⁸ or high pH conditions, where polypeptides might be uniformly charged, or not charged at all.

Ultra-fast protein recognition of peptide and protein with a nanopore is another challenge that already started. The first attempts focused on the detection and discrimination of native proteins either outside^{7,22,23,56,59} or inside^{21,29,35,38,39} the nanopore. Then an approach towards protein sequencing was to unfold the native protein and to try to read the polypeptide

sequence into the nanopore during the translocation process. An interesting work demonstrated protein unfolding and translocation through a biological nanopore using an unfoldase molecular motor (ClpX variant)²⁷. The ionic current trace during protein translocation did not allow to detect single amino-acid differences along the polypeptide sequence but showed electrical signal differences according to various protein domains with a maximum resolution of ≈ 663 amino acids⁷⁰. Up to now, unfolded protein transport through a biological nanopore was too fast to read the protein sequence^{18,48}. Recently a subnanometre diameter pore was manufactured, from a silicon nitride membrane, to indirectly read the primary sequence of an unfolded protein with a resolution of blocks of four amino acids, based on a theoretical excluded volume model⁷¹. So far, solid-state nanopores still suffer from a poorly reproducible manufacturing process and from insufficient wetting surface control. Here, in contrast, production of recombinant biological nanopores is standardized and highly reproducible. The electrical signal measurements to detect the size of short peptides with a single amino acid resolution and to discriminate between different chemical natures of homo- and heteropeptides are also highly reproducible. The high current blockade depth resolution -single amino acid- combined with the high temporal resolution -up to 10 ms/amino acid, i.e., a 3 orders of magnitude improvement as compared to previous published data¹⁸- of our system pave the road for the construction of a sequence library of all the different amino acids. As a first perspective, coupling the detection and identification of individual amino acids of different chemical nature either with the controlled translocation of an unfolded peptide/protein or with the sequential degradation of a peptide/protein near the nanopore entrance, would provide a new tool for peptide/protein sequencing. As a second perspective, combining the single-molecule sensitivity of the nanopore technology with a nanofluidic device guiding a single cell to the nanopore entrance would allow to quantify very small quantities of peptide biomarkers in a single cell. For instance, recently, Maglia and co-workers analyzed model peptide and protein biomarkers through FraC nanopores³⁸. This might lead to important advances in the field of single-molecule proteomics. Our results and those of more recent works^{37-39,59,72} pave the road to analyse realistic samples, such as those from blood stream, serum, biopsies, or lysate extracts.

Methods

Synthesis of the aerolysin nanopore. The aerolysin nanopore is a pore-forming toxin from *Aeromonas hydrophila* which forms an heptameric β -barrel pore assembly in cell membranes⁷³. The atomistic structure of aerolysin was recently defined⁷⁴. It has an inner pore diameter of 1.0–1.7 nm and has a high number of charged residues (91 charges) pointing into the pore lumen⁷⁴. Recombinant wild-type pro-aerolysin was synthesized using the following procedure. We transformed *Escherichia coli* BL21 strain with pET22b-proAL plasmid containing pro-aerolysin sequence. This plasmid allowed the induction of pro-aerolysin production with IPTG (1 mM final concentration) and the periplasmic localization of the recombinant protein. The periplasm was extracted with an osmotic shock and pro-aerolysin was furthermore purified by affinity chromatography using the C-

Fig. 4 Real-time monitoring of the enzymatic degradation of an arginine peptide sample. Scatter plot of blockade duration versus relative blockade current I_b/I_0 (top of each subfigure) and histogram of the relative blockade current I_b/I_0 values (bottom of each subfigure) in the case of the interaction of aerolysin nanopore with a solution of 9 amino acids long arginine peptides: **a** in absence of trypsin enzyme, **b** 10 min after trypsin addition and **(c)** 3 h 30 min after trypsin addition. Colored numbers on top of subfigure **(a)** indicate the number of amino acids corresponding to each blockade population. In absence of trypsin, the overwhelming majority of blockades corresponds to 9 amino acids long peptides. Only 10 min after trypsin addition, a significant (≈ 3 folds) decrease of the proportion of blockades corresponding to 9 amino acids long peptides is observed, in favor of a significant increase of the proportion of blockades corresponding to shorter peptides, indicating the trypsin cleavage of long peptides into shorter ones. In particular, the increase of the proportion of blockades with $I_b/I_0 \approx 0.73$ (gray) confirms that this population corresponds to 4 amino acids long peptides. After 3 h 30 min of trypsin activity, the 9, 8, and 7 amino acids long peptides populations have disappeared. The data were acquired in KCl 4 M HEPES 5 mM pH = 7.5 at -50 mV and at 20 °C

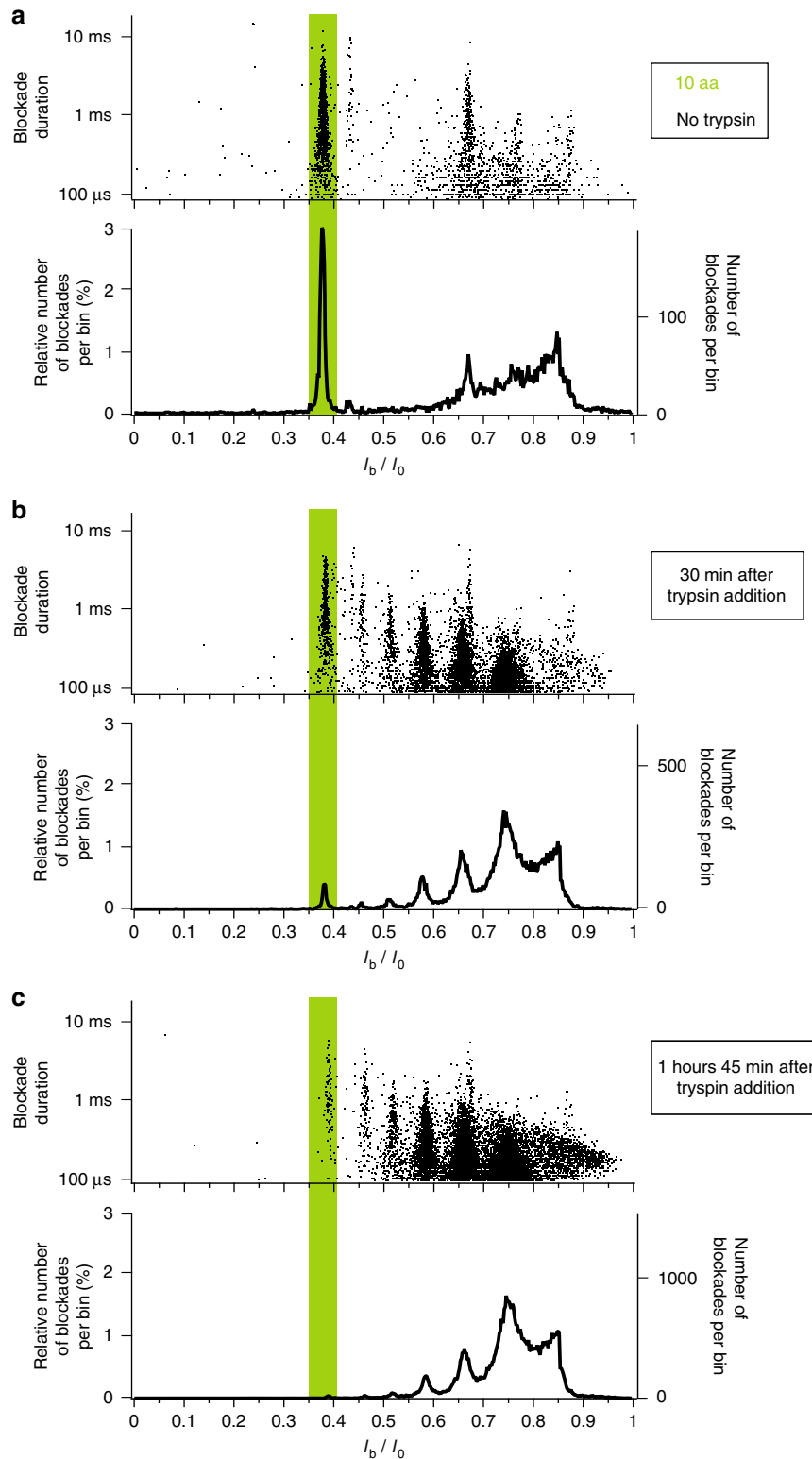


Fig. 5 Real-time monitoring of the enzymatic degradation of a lysine peptide sample. Scatter plot of blockade duration versus relative blockade current I_b/I_0 (top of each subfigure) and histogram of the relative blockade current I_b/I_0 values (bottom of each subfigure) in the case of the interaction of aerolysin nanopore with a solution of 10 amino acids long lysine peptides: **a** in absence of trypsin enzyme, **(b)** 30 min after trypsin addition, and **(c)** 1 h 45 min after trypsin addition. In absence of trypsin, the majority of blockades corresponds to 10 amino acids long peptides. After trypsin addition, a significant decrease of the proportion of blockades corresponding to 10 amino acids long peptides is observed, in favor of a significant increase of the proportion of blockades corresponding to shorter peptides, indicating the trypsin cleavage of long peptides into shorter ones. The data were acquired in KCl 4 M HEPES 5 mM pH = 7.5 at -50 mV and at 20°C

terminal his-tag of the recombinant protein (His SpinTrap minicolumns, GE Healthcare Life Science). Pro-aerolysin binding to the Ni-Sepharose was made with 100 mM Tris-HCl pH 7.4 and 50 mM imidazole, and after three washing steps, elution was made with 100 mM Tris-HCl pH 7.4 and 500 mM imidazole. The recombinant pro-aerolysin purity was determined by SDS-polyacrylamide gel electrophoresis and Coomassie bleu staining, to $99 \pm 1\%$ (w/w). Concentration was calculated by absorbance at 280 nm. The propeptides of pro-aerolysin monomers were stored at 4 °C at a final concentration of 0.1 g/L.

Nanopore recordings. A classical vertical lipid bilayer setup (Warner Instruments, Hamden, CT, USA or Elements, Cesena (FC), Italy) was used for all the experiments. The lipid bilayer was formed by painting and thinning a film of diphytanoyl-phosphocholine (Avanti Polar Lipids, Alabaster, AL, USA) dissolved in decane (10 mg/mL) over a 150 μm -wide aperture separating the *cis* and *trans* chambers. Both chambers were filled with 1 mL of 4 M KCl solution buffered with 5 mM HEPES and set to pH = 7.5. Two Ag/AgCl electrodes were used to apply a transmembrane voltage and to measure the transmembrane ionic current. The *cis*-chamber was at voltage ground.

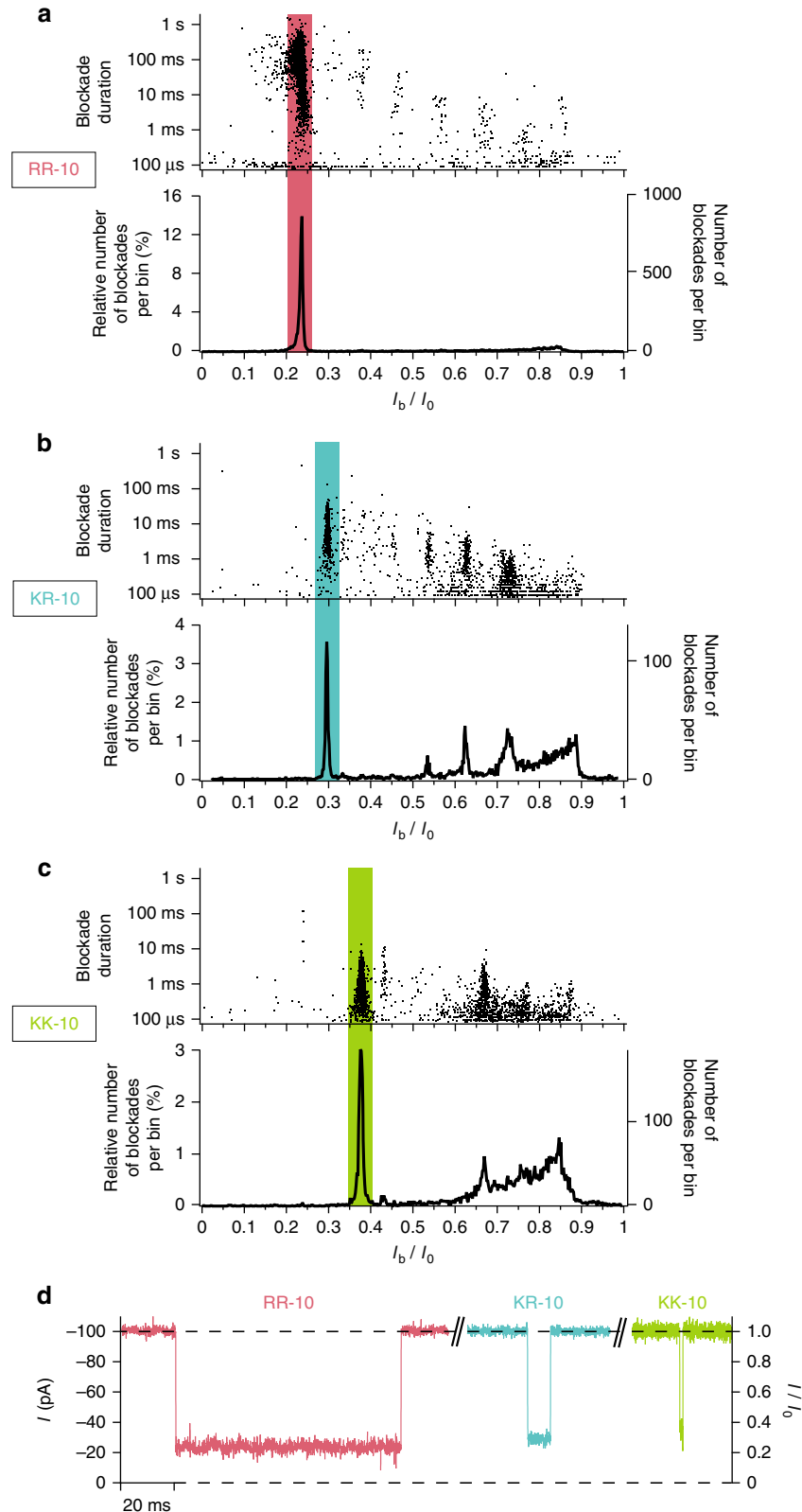


Fig. 6 Discrimination of 10 amino acids long peptides of different sequences. **a–c** Scatter plot of blockade duration versus relative blockade current I_b/I_0 (top of each subfigure) and histogram of the relative blockade current I_b/I_0 values (bottom of each subfigure) in the case of the interaction of aerolysin nanopore with: **(a)** a solution of 10 amino acids long arginine homopeptides (RRRRRRRRR, named RR-10), **(b)** a solution of 10 amino acids long lysine/arginine heteropeptides (KKKKRRRRR, named KR-10) and **(c)** a solution of 10 amino acids long lysine homopeptides (KKKKKKKKK, named KK-10). Each histogram corresponding to a given peptide sequence exhibits a main I_b/I_0 population clearly distinct from the other peptide sequences, allowing to discriminate between peptides of same length but of different sequences. **d** Typical current blockades in the case of the interaction of aerolysin nanopore with (from left to right) a solution of RR-10 peptides, with a solution of KR-10 peptides and with a solution of KK-10 peptides. The left axis indicates the current I values (negative current values under a negative applied voltage) and the right axis indicates the relative current I/I_0 values. For each peptide sequence, the typical current blockade has a relative blockade current I_b/I_0 value and a blockade duration respectively equal to the mean I_b/I_0 value and to the mean blockade duration of the main population of the histograms shown in **(a–c)** (see also Supplementary Fig. 7). The data were acquired in KCl 4 M HEPES 5 mM pH = 7.5 at -50 mV and at 20 °C

In the case of the Warner Instruments setup, single-channel current recordings were performed using an Axopatch 200B patch-clamp amplifier (Molecular Devices, Sunnyvale, CA, USA) in the whole-cell mode with a CV-203BU headstage. The signal was filtered using an internal 4-pole Bessel filter at a cut-off frequency of 5 kHz. Data were acquired with a DigiData 1440A AD-converter (Molecular Devices) controlled by the Clampex 10.2 software (Molecular Devices). Current recordings at constant voltage were performed at a sampling rate of 250 kHz. Current versus voltage recordings were performed from -100 to $+100$ mV during 4 s and at a sampling rate of 5 kHz. A Peltier device controlled by a bipolar temperature controller (CL-100, Warner Instruments) allowed to set the temperature of the solution via a water circuit (LCS-1, Warner Instruments) around the chambers. The temperature was set to 20.0 ± 2 °C for all the experiments.

In the case of the Elements setup, single-channel current recordings were performed using an eONE amplifier (Elements, Cesena (FC), Italy). The signal was filtered at a cut-off frequency of 5 kHz. Data were acquired using the Elements Data Reader software (Elements, Cesena (FC), Italy), at a sampling rate of 200 kHz.

Recombinant wild-type pro-aerolysin was activated by trypsin digestion (0.6 μ M trypsin final concentration) during 15 min at room temperature to eliminate the pro-peptide sequence. After the formation of the lipid bilayer, activated aerolysin was added to the *cis*-chamber at ≈ 1 nM final concentration. The insertion of a single nanopore in the lipid bilayer was identified as a step-jump of the transmembrane ionic current.

High-purity (>98%) arginine homopeptide samples (ProteoGenix, Schiltigheim, France) of different lengths (3, 5, 6, 7, 8, 9, 10, 12 amino acids) were used. Peptides were dissolved in aqueous 5 mM HEPES pH = 7.5 buffer. In the case of current recordings at constant voltage, peptides were added to the *cis*-chamber, either as a 1 μ M equimolar mixture of peptides of different lengths or as a 1 μ M solution of peptides of a given length. In the case of current versus voltage recordings, 10 amino acids long peptides were added either to the *trans*-chamber at a 6 μ M concentration, or to the *cis*-chamber at a 1.2 μ M concentration (Supplementary Fig. 1). In each case, after peptide addition, a ≈ 2 mL mixing of the volume of the chamber corresponding to the side of peptide addition was performed, and a ≈ 10 min waiting time was observed in order to ensure an homogeneous peptide concentration in the chamber.

The enzymatic degradation of arginine homopeptides was performed by adding trypsin at 25 nM final concentration to a 4.4 μ M solution of 9 amino acids long peptides. Ten minutes current recordings were performed every 10 min after trypsin addition, during 3 h 30 min.

High-purity (>98%) lysine homopeptide samples (ProteoGenix, Schiltigheim, France) of 10 amino acids were used. Peptides were dissolved in aqueous 5 mM HEPES pH = 7.5 buffer. Peptides were added to the *cis*-chamber as a 213 μ M solution of peptides. After peptide addition, a ≈ 2 mL mixing of the volume of the chamber corresponding to the side of peptide addition was performed, and a ≈ 10 min waiting time was observed in order to ensure an homogeneous peptide concentration in the chamber.

The enzymatic degradation of lysine homopeptides was performed by adding trypsin at 266 nM final concentration to a 213 μ M solution of 10 amino acids long peptides. 5 min current recordings were performed every 5 min after trypsin addition, during 1 h 45 min.

High-purity (>98%) lysine/arginine heteropeptide samples (ProteoGenix, Schiltigheim, France) of 10 amino acids were used. Peptides were dissolved in aqueous 5 mM HEPES pH = 7.5 buffer. Peptides were added to the *cis*-chamber as a 1 μ M solution of peptides. After peptide addition, a ≈ 2 mL mixing of the volume of the chamber corresponding to the side of peptide addition was performed, and a ≈ 10 min waiting time was observed in order to ensure an homogeneous peptide concentration in the chamber.

Data treatment. The data treatment was performed using the Igor Pro 6.12A software (WaveMetrics, Portland, OR, USA) with homemade procedures. The treatment was based on a statistical analysis of a least 2000 blockade events for each current trace. A two-thresholds method was used to detect peptide-induced current blockades (Supplementary Fig. 8). A first threshold $th_1 = I_0 - 4\sigma$ was used to define

every possible blockade event, where I_0 and σ are respectively the mean open pore current and its standard deviation obtained from a gaussian fit of the open pore current distribution. A possible blockade event begins when the pore current decreases below th_1 and ends when the pore current increases above th_1 . This first threshold allows to eliminate the overwhelming part of the open pore current noisy fluctuations. If the mean blockade current value I_b during the event is inferior to a second threshold $th_2 = I_0 - 5\sigma$, then the event is considered as a peptide-induced blockade event.

Histograms of the relative blockade current I_b/I_0 values were obtained using a bin width of 0.002. For each peptide length, the mean relative blockade current value $\langle I_b/I_0 \rangle_i$ ($i = 5, 6, 7, 8, 9$, or 10 amino acids long peptides) corresponds to the mean value of a gaussian fit of the I_b/I_0 peak corresponding to this peptide length. The error bar of each $\langle I_b/I_0 \rangle_i$ corresponds to the standard deviation σ_i of the gaussian fit of the peak. The current blockades corresponding to each peptide length were identified as the current blockades with I_b/I_0 values comprised between $\langle I_b/I_0 \rangle_i - 3\sigma_i$ and $\langle I_b/I_0 \rangle_i + 3\sigma_i$. From the current blockades corresponding to each peptide length, the mean blockade duration and frequency were calculated for each peptide length. The mean blockade duration is the mean value of: the calculated mean value of blockade durations, the mean blockade duration obtained from a single exponential fit of the blockade durations distribution and the mean blockade duration obtained from a single exponential fit of the cumulative blockade durations distribution (Supplementary Fig. 9). The error bar of the mean blockade duration is the maximal value among: the sampling time interval of the acquisition system (4 μ s at 250 kHz sampling rate), the dispersion of the mean blockade durations obtained from the 3 methods above and the standard deviation of the fit coefficients from the data analysis software. The same procedure applied to the inter-blockade durations provided the mean inter-blockade duration, and thus the mean blockade frequency, and its error bar for each peptide length.

The results were reproduced with a high fidelity from at least 4 independent experiments (Supplementary Fig. 4). The results presented in this article correspond to individual experiments.

Data availability. The authors declare that the data supporting the findings of this study are available within the article and its Supplementary Information files or from the corresponding authors upon reasonable request.

Received: 5 October 2017 Accepted: 9 February 2018

Published online: 06 March 2018

References

- Lee, K.-E., Heo, J.-E., Kim, J.-M. & Hwang, C.-S. N-terminal acetylation-targeted N-end rule proteolytic system: the Ac/N-end rule pathway. *Mol. Cells* **39**, 169–178 (2016).
- Shao, S. et al. Minimal sample requirement for highly multiplexed protein quantification in cell lines and tissues by PCT-SWATH mass spectrometry. *Proteomics* **15**, 3711–3721 (2015).
- Schubert, O. T., Röst, H. L., Collins, B. C., Rosenberger, G. & Aebersold, R. Quantitative proteomics: challenges and opportunities in basic and applied research. *Nat. Protoc.* **12**, 1289–1294 (2017).
- Swietlow, A. & Lax, R. Quality control in peptide manufacturing: specifications for GMP peptides. *Chim. Oggi.* **22**, 22–24 (2004).
- Kasianowicz, J. J., Brandin, E., Branton, D. & Deamer, D. W. Characterization of individual polynucleotide molecules using a membrane channel. *Proc. Natl Acad. Sci. USA* **93**, 13770–13773 (1996).
- Venkatesan, B. M. & Bashir, R. Nanopore sensors for nucleic acid analysis. *Nat. Nanotechnol.* **6**, 615–624 (2011).
- Movileanu, L., Howorka, S., Braha, O. & Bayley, H. Detecting protein analytes that modulate transmembrane movement of a polymer chain within a single protein pore. *Nat. Biotechnol.* **18**, 1091–1095 (2000).

8. Sutherland, T. C. et al. Structure of peptides investigated by nanopore analysis. *Nano. Lett.* **4**, 1273–1277 (2004).
9. Movileanu, L., Schmittschmitt, J. P., Scholtz, J. M. & Bayley, H. Interactions of peptides with a protein pore. *Biophys. J.* **89**, 1030–1045 (2005).
10. Stefureac, R., Long, Y.-T., Kraatz, H.-B., Howard, P. & Lee, J. S. Transport of alpha-helical peptides through alpha-hemolysin and aerolysin pores. *Biochemistry* **45**, 9172–9179 (2006).
11. Cheley, S., Xie, H. & Bayley, H. A genetically encoded pore for the stochastic detection of a protein kinase. *ChemBiochem* **7**, 1923–1927 (2006).
12. Oukhaled, G. et al. Unfolding of proteins and long transient conformations detected by single nanopore recording. *Phys. Rev. Lett.* **98**, 158101 (2007).
13. Wolfe, A. J., Mohammad, M. M., Cheley, S., Bayley, H. & Movileanu, L. Catalyzing the translocation of polypeptides through attractive interactions. *J. Am. Chem. Soc.* **129**, 14034–14041 (2007).
14. Goodrich, C. P. et al. Single-molecule electrophoresis of beta-hairpin peptides by electrical recordings and Langevin dynamics simulations. *J. Phys. Chem. B.* **111**, 3332–3335 (2007).
15. Zhao, Q., de Zoysa, R. S. S., Wang, D., Jayawardhana, D. A. & Guan, X. Real-time monitoring of peptide cleavage using a nanopore probe. *J. Am. Chem. Soc.* **131**, 6324–6325 (2009).
16. Bikwemu, R., Wolfe, A. J., Xing, X. & Movileanu, L. Facilitated translocation of polypeptides through a single nanopore. *J. Phys. Condens. Matter* **22**, 454117 (2010).
17. Kukwikila, M. & Howorka, S. Electrically sensing protease activity with nanopores. *J. Phys. Condens. Matter* **22**, 454103 (2010).
18. Pastoriza-Gallego, M. et al. Dynamics of unfolded protein transport through an aerolysin pore. *J. Am. Chem. Soc.* **133**, 2923–2931 (2011).
19. Mahendran, K. R., Romero-Ruiz, M., Schlöisinger, A., Winterhalter, M. & Nussberger, S. Protein translocation through Tom40: kinetics of peptide release. *Biophys. J.* **102**, 39–47 (2012).
20. Singh, P. R. et al. Pulling peptides across nanochannels: resolving peptide binding and translocation through the hetero-oligomeric channel from *Nocardia farcinica*. *ACS Nano* **6**, 10699–10707 (2012).
21. Soskine, M. et al. An engineered ClyA nanopore detects folded target proteins by selective external association and pore entry. *Nano. Lett.* **12**, 4895–4900 (2012).
22. Rotem, D., Jayasingh, L., Salichou, M. & Bayley, H. Protein detection by nanopores equipped with aptamers. *J. Am. Chem. Soc.* **134**, 2781–2787 (2012).
23. Mohammad, M. M. et al. Engineering a rigid protein tunnel for biomolecular detection. *J. Am. Chem. Soc.* **134**, 9521–9531 (2012).
24. Payet, L. et al. Thermal unfolding of proteins probed at the single molecule level using nanopores. *Anal. Chem.* **84**, 4071–4076 (2012).
25. Lamichhane, U. et al. Peptide translocation through the mesoscopic channel: Binding kinetics at the single molecule level. *Eur. Biophys. J.* **42**, 363–369 (2013).
26. Mahendran, K. R., Lamichhane, U., Romero-Ruiz, M., Nussberger, S. & Winterhalter, M. Polypeptide translocation through the mitochondrial TOM channel: temperature-dependent rates at the single-molecule level. *J. Phys. Chem. Lett.* **4**, 78–82 (2013).
27. Nivala, J., Marks, D. B. & Akeson, M. Unfoldase-mediated protein translocation through an α -hemolysin nanopore. *Nat. Biotechnol.* **31**, 247–250 (2013).
28. Soskine, M., Biesemans, A., De Maeyer, M. & Maglia, G. Tuning the size and properties of clyA nanopores assisted by directed evolution. *J. Am. Chem. Soc.* **135**, 13456–13463 (2013).
29. Van Meervelt, V., Soskine, M. & Maglia, G. Detection of two isomeric binding configurations in a protein-aptamer complex with a biological nanopore. *ACS Nano* **8**, 12826–12835 (2014).
30. Mereuta, L. et al. Slowing down single-molecule trafficking through a protein nanopore reveals intermediates for peptide translocation. *Sci. Rep.* **4**, 3885 (2014).
31. Pastoriza-Gallego, M. et al. Evidence of unfolded protein translocation through a protein nanopore. *ACS Nano* **8**, 11350–11360 (2014).
32. Fahie, M., Chisholm, C. & Chen, M. Resolved single-molecule detection of individual species within a mixture of anti-biotin antibodies using an engineered monomeric nanopore. *ACS Nano* **9**, 1089–1098 (2015).
33. Biesemans, A., Soskine, M. & Maglia, G. A protein rotaxane controls the translocation of proteins across a ClyA nanopore. *Nano. Lett.* **15**, 6076–6081 (2015).
34. Soskine, M., Biesemans, A. & Maglia, G. Single-molecule analyte recognition with ClyA nanopores equipped with internal protein adaptors. *J. Am. Chem. Soc.* **137**, 5793–5797 (2015).
35. Ji, Z. et al. Fingerprinting of peptides with a large channel of bacteriophage Phi29 DNA packaging motor. *Small* **12**, 4572–4578 (2016).
36. Hu, Y.-X. et al. Single molecule study of initial structural features on the amyloidosis process. *Chem. Commun.* **52**, 5542–5545 (2016).
37. Chavis, A. E. et al. Single molecule nanopore spectrometry for peptide detection. *ACS Sensors* **2**, (1319–1328 (2017)).
38. Huang, G., Willems, K., Soskine, M., Wloka, C. & Maglia, G. Electro-osmotic capture and ionic discrimination of peptide and protein biomarkers with FraC nanopores. *Nat. Commun.* **8**, 935 (2017).
39. Van Meervelt, V. et al. Real-time conformational changes and controlled orientation of native proteins inside a protein nanoreactor. *J. Am. Chem. Soc.* **139**, 18640–18646 (2017).
40. Han, A. et al. Sensing protein molecules using nanofabricated pores. *Appl. Phys. Lett.* **88**, 093901 (2006).
41. Uram, J. D., Ke, K., Hunt, A. J. & Mayer, M. Label-free affinity assays by rapid detection of immune complexes in submicrometer pores. *Angew. Chem., Int. Ed.* **45**, 2281–2285 (2006).
42. Sexton, L. T. et al. Resistive-pulse studies of proteins and protein/antibody complexes using a conical nanotube sensor. *J. Am. Chem. Soc.* **129**, 13144–13152 (2007).
43. Fologea, D., Ledden, B., McNabb, D. S. & Li, J. Electrical characterization of protein molecules by a solid-state nanopore. *Appl. Phys. Lett.* **91**, 053901 (2007).
44. Talaga, D. S. & Li, J. Single-molecule protein unfolding in solid state nanopores. *J. Am. Chem. Soc.* **131**, 9287–9297 (2009).
45. Firnkes, M., Pedone, D., Knezevic, J., Döblinger, M. & Rant, U. Electrically facilitated translocations of proteins through silicon nitride nanopores: conjoint and competitive action of diffusion, electrophoresis, and electroosmosis. *Nano Lett.* **10**, 2162–2167 (2010).
46. Oukhaled, A. et al. Dynamics of completely unfolded and native proteins through solid-state nanopores as a function of electric driving force. *ACS Nano* **5**, 3628–3638 (2011).
47. Yusko, E. C. et al. Controlling protein translocation through nanopores with bio-inspired fluid walls. *Nat. Nanotechnol.* **6**, 253–260 (2011).
48. Cressiot, B. et al. Protein transport through a narrow solid-state nanopore at high voltage: experiments and theory. *ACS Nano* **6**, 6236–6243 (2012).
49. Japrun, D. et al. Single-molecule studies of intrinsically disordered proteins using solid-state nanopores. *Anal. Chem.* **85**, 2449–2456 (2013).
50. Freedman, K. J., Haq, S. R., Edell, J. B., Jemth, P. & Kim, M. J. Single molecule unfolding and stretching of protein domains inside a solid-state nanopore by electric field. *Sci. Rep.* **3**, 1638 (2013).
51. Li, W. et al. Single protein molecule detection by glass nanopores. *ACS Nano* **7**, 4129–4134 (2013).
52. Rosen, C. B., Rodriguez-Larrea, D. & Bayley, H. Single-molecule site-specific detection of protein phosphorylation with a nanopore. *Nat. Biotechnol.* **32**, 179–181 (2014).
53. Steinbock, L. J. et al. Probing the size of proteins with glass nanopores. *Nanoscale* **6**, 14380–14387 (2014).
54. Nir, I., Huttner, D. & Meller, A. Direct sensing and discrimination among ubiquitin and ubiquitin chains using solid-state nanopores. *Biophys. J.* **108**, 2340–2349 (2015).
55. Balme, S. et al. Influence of adsorption on proteins and amyloids detection by silicon nitride nanopore. *Langmuir* **32**, 8916–8925 (2016).
56. Bell, N. A. W. & Keyser, U. F. Digitally encoded DNA nanostructures for multiplexed, single-molecule protein sensing with nanopores. *Nat. Nanotechnol.* **11**, 645–651 (2016).
57. Waduge, P. et al. Nanopore-based measurements of protein size, fluctuations, and conformational changes. *ACS Nano* **11**, 5706–5716 (2017).
58. Wloka, C. et al. Label-free and real-time detection of protein ubiquitination with a biological nanopore. *ACS Nano* **11**, 4387–4394 (2017).
59. Sze, J. Y. Y., Ivanov, A. P., Cass, A. E. G. & Edell, J. B. Single molecule multiplexed nanopore protein screening in human serum using aptamer modified DNA carriers. *Nat. Commun.* **8**, 1552 (2017).
60. Xie, H., Braha, O., Gu, L.-Q., Cheley, S. & Bayley, H. Single-molecule observation of the catalytic subunit of camp-dependent protein kinase binding to an inhibitor peptide. *Chem. Biol.* **12**, 109–120 (2005).
61. Kukwikila, M. & Howorka, S. Nanopore-based electrical and label-free sensing of enzyme activity in blood serum. *Anal. Chem.* **87**, 9149–9154 (2015).
62. Rodriguez-Larrea, D. & Bayley, H. Multistep protein unfolding during nanopore translocation. *Nat. Nanotechnol.* **8**, 288–295 (2013).
63. Yusko, E. C. et al. Real-time shape approximation and fingerprinting of single proteins using a nanopore. *Nat. Nanotechnol.* **12**, 360–367 (2016).
64. Vercoutere, W. et al. Rapid discrimination among individual DNA hairpin molecules at single-nucleotide resolution using an ion channel. *Nat. Biotechnol.* **19**, 248–252 (2001).
65. Robertson, J. W. F. et al. Single-molecule mass spectrometry in solution using a solitary nanopore. *Proc. Natl Acad. Sci. USA* **104**, 8207–8211 (2007).
66. Baaken, G. et al. High-resolution size-discrimination of single nonionic synthetic polymers with a highly charged biological nanopore. *ACS Nano* **9**, 6443–6449 (2015).
67. Piguet, F. et al. High temperature extends the range of size discrimination of nonionic polymers by a biological nanopore. *Sci. Rep.* **6**, 38675 (2016).

68. Cao, C. et al. Discrimination of oligonucleotides of different lengths with a wild-type aerolysin nanopore. *Nat. Nanotechnol.* **11**, 713–718 (2016).
69. Lairez, D., Pauthe, E. & Pelta, J. Refolding of a high molecular weight protein: salt effect on collapse. *Biophys. J.* **84**, 3904–3916 (2003).
70. Nivala, J., Mulrone, L., Li, G., Schreiber, J. & Akeson, M. Discrimination among protein variants using an unfoldase-coupled nanopore. *ACS Nano* **8**, 12365–12375 (2014).
71. Kennedy, E., Dong, Z., Tennant, C. & Timp, G. Reading the primary structure of a protein with 0.07 nm³ resolution using a subnanometre-diameter pore. *Nat. Nanotechnol.* **11**, 968–976 (2016).
72. Xi, D., Li, Z., Liu, L., Ai, S. & Zhang, S. Ultrasensitive detection of cancer cells combining enzymatic signal amplification with an aerolysin nanopore. *Anal. Chem.* **90**, 1029–1034 (2018).
73. Parker, M. W. et al. Structure of the *Aeromonas* toxin proaerolysin in its water-soluble and membrane-channel states. *Nature* **367**, 292–295 (1994).
74. Degiacomi, M. T. et al. Molecular assembly of the aerolysin pore reveals a swirling membrane-insertion mechanism. *Nat. Chem. Biol.* **9**, 623–629 (2013).

Acknowledgements

This work was supported by grants from the Agence Nationale de la Recherche (ANR-17-CE09-0032-01 to F.P., M.P.-G., and A.O.; ANR-17-CE09-0044-02 to P.M., M.P.-G., A.O., and J.P.; ANR12-NANO-0012-03, to J.P. and A.O.), and from the Région Ile-de-France in the framework of DIM Nano-K (n° 094251, to A.O.). This work was also supported by the Direction Générale de l'Armement (the French Defense Procurement Agency, n° 2017 60 0042 to H.O. and A.O.) and by the Région Ile-de-France in the framework of DIM ResPore (n° 2017-05 to H.O. and A.O.). We thank Excilone company (France) which provided financial support to H.O. We thank F. Gisou van der Goot (Ecole Polytechnique Fédérale de Lausanne, Switzerland) which generously provided the pET22b-proAL plasmid containing the pro-aerolysin sequence. We thank Guillaume Lamour (Université d'Evry-Val-d'Essonne) for careful reading and for improving the use of English in the manuscript.

Author contributions

J.P. and A.O. conceived the project. A.O. managed the project, designed the nanopore platform, and conceived the experiments. M.P.-G. produced the recombinant wild-type

pro-aerolysin. F.P., H.O., and A.O. performed the experiments and analyzed the data. All authors participated to the interpretation of the data. F.P., H.O., and A.O. prepared the manuscript figures. F.P., H.O., P.M., J.P., and A.O. wrote the manuscript. All authors reviewed the manuscript.

Additional information

Supplementary Information accompanies this paper at <https://doi.org/10.1038/s41467-018-03418-2>.

Competing interests: F.P., H.O., P.M., J.P., and A.O. are named as inventors in a patent application (Institut National de la Propriété Industrielle patent application number 16/01007, European patent application number EP17177951.5, Patent Cooperation Treaty application number 17/000129). M.P.-G. declares no competing interests.

Reprints and permission information is available online at <http://npg.nature.com/reprintsandpermissions/>

Publisher's note: Springer Nature remains neutral with regard to jurisdictional claims in published maps and institutional affiliations.



Open Access This article is licensed under a Creative Commons Attribution 4.0 International License, which permits use, sharing, adaptation, distribution and reproduction in any medium or format, as long as you give appropriate credit to the original author(s) and the source, provide a link to the Creative Commons license, and indicate if changes were made. The images or other third party material in this article are included in the article's Creative Commons license, unless indicated otherwise in a credit line to the material. If material is not included in the article's Creative Commons license and your intended use is not permitted by statutory regulation or exceeds the permitted use, you will need to obtain permission directly from the copyright holder. To view a copy of this license, visit <http://creativecommons.org/licenses/by/4.0/>.

© The Author(s) 2018